Int. J. Heat Mass Transfer. Vol. 30, No. 3, pp. 527 535, 1987
Printed in Great Britain

0017-9310/87 $3.00 + 0.00
Pergamon Journals Ltd.

Fluid flow and heat transfer in the duct of an MHD power generator

M. L. MITTAL, H. R. NATARAJA and V. G. NAIDU
Department of Mathematics, Indian Institute of Technology, Powai, Bombay 400076, India

(*Received* 22 *April* 1985)

Abstract—A numerical solution of the equations governing the flow of an electrically conducting, viscous, compressible gas with variable fluid properties in the presence of a uniform magnetic field is obtained. The velocity and temperature distributions for subsonic and supersonic flows as these occur in the duct of an MHD generator are analysed.

INTRODUCTION

THE PROBLEM of fluid flow and heat transfer in the duct of a magnetohydrodynamic (MHD) power generator, while important for the calculations of almost all the characteristics of the generator, is rather complex for analytical solutions. The governing equations are coupled nonlinear equations and probably because of this reason, the attempts in this direction are meagre although experimental studies have been made by several authors [1–3] to understand the flow behaviour.

Earlier, calculations for electric current density, power, efficiency, etc. were made using the one-dimensional form of the averaged governing equations of fluid flow and heat transfer, as was pointed out by Blackman *et al.* [4],

> It is impossible to solve completely the MHD generator problem including viscosity, compressibility, heat transfer, nonscalar conductivity, etc. As a compromise, however, one can consider briefly the status of a 'model' which in the literature of MHD power production (one-dimensional hydraulic calculations) has been judged as an adequate starting point for engineering calculations.

But these assumptions obliterate most of the important features of the problem and do not give an account of various losses due to viscous and thermal boundary layers.

Later, to study the effect of viscous boundary layer on electric current and potential distribution and other characteristics of the generator, some authors used a boundary-layer-type velocity profile [5, 6] based on the empirical relation. This empirical relation gives the behaviour of velocity as a function of the normal distance, if one knows the boundary-layer thickness of the flow *a priori* and if this does not vary with any other fluid property or channel configuration. Besides other weaknesses, this type of velocity and temperature profiles have gradients which are discontinuous on the boundary, and hence the conclusions based on the studies using these profiles would be doubtful.

Doss *et al.* [7] have made claims to have developed some computer codes for generating the velocity and temperature profiles. But neither their solutions nor any other method for solution is available in the published literature. Gertz *et al.* [8] have given another approximate representation for these profiles using momentum integral method. Vanka and Ahluwalia [9] have obtained the approximate solution which should predict three-dimensional flow and thermal development in MHD channels based on the calculation procedure suggested by Patankar *et al.* [10] for three-dimensional hydrodynamic parabolic flows.

In this paper, the numerical solutions of the equations governing the laminar fluid flow and heat transfer in the boundary-layer region of the electrode walls of the duct of an MHD generator are presented. The method used is an improvement over the Patankar and Spalding [11] technique as modified by Arad *et al.* [12] for the solution of boundary-layer equations for viscous compressible fluids without magnetic field. The strong Joule heating effects in the boundary-layer region over the electrode walls add to the difficulties of the numerical solution of these equations. In this case, the gradients get sharper and therefore the solution procedure followed in hydrodynamic flows cannot be directly used for MHD flows with large interaction parameter. It is probably due to this reason that Vanka and Ahluwalia [9] in their analysis have considered a subsonic flow with small interaction parameter.

The numerical solutions giving velocity and temperature profiles are analysed for combustion product plasma and argon–potassium plasma which are the usual working fluids for open-cycle and closed-cycle generators, respectively. These plasmas are treated as a partially ionized gas with variable fluid properties like viscosity, thermal conductivity, electrical conductivity, etc. For combustion product plasma, a supersonic flow with high interaction parameter is considered, while for argon–potassium plasma a subsonic flow is considered.

NOMENCLATURE

B_0	applied magnetic field
E_x, E_y	electric field components
H	height of the channel
I	interaction parameter, $L\sigma_0 B_0^2/\rho_0 u_0$
J	current density
K	load parameter
L	characteristic length
M	Mach number
Nu	Nusselt number, $-(k\,\partial T/\partial y)_{y=0}/k_\infty(T_w - T_\infty)$
Pr	Prandtl number, $\mu_0 c_p/k_0$
Re	Reynolds number, $LU_0\rho_0/\mu_0$
T	temperature
c_p	specific heat at constant pressure
c_v	specific heat at constant volume
h	enthalpy
k	thermal conductivity
p	pressure
u, v	velocity components.

Greek symbols

β_e	Hall parameter, $\omega_e\tau_e$
β_i	ion slip parameter, $\omega_i\tau_i$
γ	ratio of specific heats
δ	boundary-layer thickness
η, ω, λ	dimensionless Cartesian coordinates
τ	shear stress
ψ	streamfunction
ρ	density
μ	dynamic viscosity
σ	electrical conductivity.

Subscripts

g	gas
w	wall condition
x, y	components in x, y directions
0	entrance condition
∞	free-stream condition.

MATHEMATICAL FORMULATION

Considering the flow of a viscous compressible gas in a linear MHD duct of constant cross-section, the direction of the flow is taken as the x-axis. A constant magnetic field is acting uniformly in the z-direction. The electrodes placed at $y = 0$ and $y = H$ are maintained at a uniform temperature T_w. These electrodes are connected to an external load to draw the power. The magnetic Reynolds number of the partially ionized gas as considered in the present case, is very small ($O \simeq 10^{-4}$) and hence the induced magnetic field is neglected in the analysis. The walls perpendicular to the z-axis are perfect insulators and they are separated sufficiently to make the two-dimensional analysis valid. The transport coefficients of the gas, the viscosity, thermal conductivity, electrical conductivity and Hall and ion-slip parameters are taken as functions of temperature.

For such a system, the components of velocity **V**, the magnetic field **B**, the current density **J** and the electric field **E** are

$$\mathbf{V} = (u, v, 0) \tag{1}$$

$$\mathbf{B} = (0, 0, B_0) \tag{2}$$

$$\mathbf{J} = (j_x, j_y, 0) \tag{3}$$

$$\mathbf{E} = (E_x, E_y, 0). \tag{4}$$

The equations governing such a two-dimensional, steady-state flow in nondimensional form [15] are written as

$$\frac{\partial}{\partial x}(\rho u) + \frac{\partial}{\partial y}(\rho v) = 0 \tag{5}$$

$$\rho\left(u\frac{\partial u}{\partial x} + v\frac{\partial u}{\partial y}\right) = -\frac{1}{\gamma M_0^2}\frac{\partial p}{\partial x} + \frac{1}{Re}\left[\frac{\partial}{\partial x}\left(\mu\frac{\partial u}{\partial x}\right) + \frac{\partial}{\partial y}\left(\mu\frac{\partial u}{\partial y}\right)\right] + Ij_y \tag{6}$$

$$\rho\left(u\frac{\partial v}{\partial x} + v\frac{\partial v}{\partial y}\right) = -\frac{1}{\gamma M_0^2}\frac{\partial p}{\partial y} + \frac{1}{Re}\left[\frac{\partial}{\partial x}\left(\mu\frac{\partial v}{\partial x}\right) + \frac{\partial}{\partial y}\left(\mu\frac{\partial v}{\partial y}\right)\right] - Ij_x \tag{7}$$

$$\rho\left(u\frac{\partial T}{\partial x} + v\frac{\partial T}{\partial y}\right) = \frac{\gamma - 1}{\gamma}\left(u\frac{\partial p}{\partial x} + v\frac{\partial p}{\partial y}\right) + \frac{1}{RePr}\left[\frac{\partial}{\partial x}\left(k\frac{\partial T}{\partial x}\right) + \frac{\partial}{\partial y}\left(k\frac{\partial T}{\partial y}\right)\right] + (\gamma - 1)M_0^2\left[\frac{4}{3}\frac{\mu}{Re}\left(\frac{\partial u}{\partial x} + \frac{\partial v}{\partial y}\right)^2 + \frac{\mu}{Re}\left(\frac{\partial u}{\partial y} + \frac{\partial v}{\partial x}\right)^2\right] - 4\mu\frac{(\gamma - 1)M_0^2}{Re}\frac{\partial u}{\partial x}\frac{\partial v}{\partial y} + \frac{I\alpha_e}{\sigma}\frac{j_x^2 + j_y^2}{\alpha_e^2 + \beta_e^2} \tag{8}$$

$$p = \rho T \tag{9}$$

$$j_x = \frac{\sigma}{\alpha_e^2 + \beta_e^2}[\alpha_e(E_x + v) - \beta_e(E_y - u)] \tag{10}$$

$$j_y = \frac{\sigma}{\alpha_e^2 + \beta_e^2}[\alpha_e(E_y - u) + \beta_e(E_x + v)]. \tag{11}$$

The variables u, v, p, ρ, T and the transport coefficients μ, k, σ, etc. are nondimensionalized with respect to their respective values at the inlet of the

channel denoted by the subscript zero. For spatial coordinates, L, the length of the channel, is used for this purpose. Here

$$Re = \rho_0 u_0 L/\mu_0 \tag{12}$$

$$I = \sigma_0 B_0^2 L/\rho_0 u_0 \tag{13}$$

$$Pr = \mu_0 c_p/k_0 \tag{14}$$

$$M_0^2 = \rho_0 u_0^2/\gamma p_0 \tag{15}$$

$$\alpha_e = 1 + \beta_e \beta_i. \tag{16}$$

Making the usual boundary-layer approximations that the diffusive effects (due to finite values of μ and k) are important only in a small layer of thickness $\delta \simeq O(1/\sqrt{Re})$ and

$$v, j_x \simeq O(\delta) \tag{17}$$

while

$$u, \frac{\partial p}{\partial x}, j_y \simeq O(1) \tag{18}$$

equations (5)–(8) are written as

$$\frac{\partial}{\partial x}(\rho u) + \frac{\partial}{\partial \bar{y}}(\rho \bar{v}) = 0 \tag{19}$$

$$\rho\left(u\frac{\partial u}{\partial x} + \bar{v}\frac{\partial u}{\partial \bar{y}}\right) = -\frac{1}{\gamma M_0^2}\frac{\partial p}{\partial x} + \frac{\partial}{\partial \bar{y}}\left(\mu\frac{\partial u}{\partial \bar{y}}\right) + \sigma' I(K - u) \tag{20}$$

$$\rho\left(u\frac{\partial h}{\partial x} + \bar{v}\frac{\partial h}{\partial \bar{y}}\right) = \frac{1}{Pr}\frac{\partial}{\partial \bar{y}}\left(k\frac{\partial h}{\partial \bar{y}}\right) + (\gamma - 1)M_0^2\frac{\partial}{\partial \bar{y}}\left[\left(\mu - \frac{k}{Pr}\right)\frac{\partial}{\partial \bar{y}}\left(\frac{u^2}{2}\right)\right] + (\gamma - 1)M_0^2\sigma' I K(K - u) \tag{21}$$

where

$$\bar{y} = y\sqrt{Re}, \qquad \bar{v} = v\sqrt{Re}, \qquad \sigma' = \frac{\sigma}{1 + \beta_e\beta_i}$$

and

$$h = T + (\gamma - 1)M_0^2\frac{u^2}{2}.$$

K is the load parameter defined as

$$E_y = K u_0 B_0. \tag{22}$$

These equations are solved with the boundary conditions

$$\bar{v} = u = 0, \qquad T = T_w \quad \text{at} \quad \bar{y} = 0 \tag{23}$$

$$u \to u_\infty \quad \text{and} \quad T \to T_\infty \quad \text{as} \quad \bar{y} \to \infty. \tag{24}$$

u_∞, T_∞ and $\partial p/\partial x$ are to be determined from one-dimensional equations for free-stream flow given by

$$\rho_\infty u_\infty = 1 \tag{25}$$

$$\frac{du_\infty}{dx} + \frac{1}{\gamma M_0^2}\frac{dp}{dx} = \sigma' I(K - u_\infty) \tag{26}$$

$$\frac{d}{dx}\left[T_\infty + (\gamma - 1)M_0^2\frac{u_\infty^2}{2}\right] = \sigma' I(\gamma - 1)M_0^2 K(K - u_\infty) \tag{27}$$

$$p = \rho_\infty T_\infty = T_\infty/u_\infty \tag{28}$$

and the initial conditions

$$p = \rho_\infty = u_\infty = T_\infty = 1 \quad \text{at} \quad x = 0. \tag{29}$$

The wall shear stress τ_w and the Nusselt number Nu are defined as

$$\tau_w = \left(\mu\frac{\partial u}{\partial y}\right)_{y=0} \tag{30}$$

$$c_f = \tau_w/(\rho_\infty u_\infty^2/2) \tag{31}$$

$$Nu = -\frac{(k\,\partial T/\partial y)_{y=0}}{k_\infty(T_w - T_\infty)}. \tag{32}$$

This completes the mathematical formulation of the problem assuming that the variations of μ, k, σ, β_e and β_i are known for the specified gas.

SOLUTION PROCEDURE

Parabolic equations (19)–(21) with boundary conditions (23) and (24) are solved numerically following the Patankar and Spalding [11] method with modifications.

First Von Mises' transformation is used to transform the equations in terms of (x, ψ) coordinates instead of (x, y), where the streamfunction ψ is defined as

$$\rho u = \frac{\partial \psi}{\partial y} \tag{33}$$

$$\rho v = -\frac{\partial \psi}{\partial x} \tag{34}$$

so that continuity equation is satisfied automatically. Then using the transformation

$$\omega = \frac{\psi(x, y)}{\psi_E(x)} \tag{35}$$

where $\psi_E(x) = \underset{y\to\infty}{\text{Lt}}\ \psi(x, y)$, equations (20) and (21) are written as

$$\frac{\partial \phi}{\partial x} + b\omega\frac{\partial \phi}{\partial \omega}\left(c\frac{\partial \phi}{\partial \omega}\right) + d \tag{36}$$

where

$$\phi = u, h$$

$$b = -\frac{1}{\psi_E}\frac{\partial \psi_E}{\partial x}$$

$$c = \frac{\mu \rho u}{\psi_E^2}, \frac{k}{Pr}\frac{\rho u}{\psi_E^2}$$

$$d = -\frac{1}{\rho u}\frac{1}{\gamma M_0^2}\frac{dp}{dx} + \frac{\sigma' I(K-u)}{\rho u},$$
$$(\gamma - 1)M_0^2\left[\frac{\partial}{\partial \omega}\left(\mu - \frac{k}{Pr}\right)\frac{\rho u}{\psi_E^2}\frac{\partial}{\partial \omega}\left(\frac{u^2}{2}\right) + \frac{\sigma' I K(K-u)}{\rho u}\right].$$

Although this transformation makes the domain finite ($0 \leqslant \omega \leqslant 1$), the (x, ω) coordinate system introduces a singularity in the derivative at the wall. To resolve this difficulty Berger *et al.* [18] suggested the transformation

$$\omega = \lambda^2 \tag{37}$$

so that equation (36) has the form

$$\frac{\partial \phi}{\partial x} + \frac{b}{2}\lambda\frac{\partial \phi}{\partial \lambda} = \frac{1}{2\lambda}\frac{\partial}{\partial \lambda}\left(\frac{c}{2\lambda}\frac{\partial \phi}{\partial \lambda}\right) + d. \tag{38}$$

Equation (38) can be solved using a finite-difference grid which covers all the boundary layers without wasting points in the potential area. To improve the accuracy of numerical calculations, it was suggested that one should take a denser grid in a cross direction near the wall where strong velocity gradients occur, instead of using the wall functions as suggested by Patankar and Spalding [11]. Hence a variable grid with a small mesh size near the wall is suggested. Although the transformation (x, λ) also gives a certain condensation of the mesh near the wall, this is not sufficient. Hence the following transformation from λ to η is taken:

$$\tan\left(\frac{\eta}{A}\right) = \lambda \tan\left(\frac{1}{A}\right) \tag{39}$$

where the value of the constant A is chosen judiciously to improve numerical efficiency. This is achieved by having at least half the grid points in the first percent of boundary-layer width and a reasonable number of points near the potential flow boundary.

With the new coordinate system equation (38) is transformed as

$$\frac{\partial \phi}{\partial x} + b\bar{\Lambda}\frac{\partial \phi}{\partial \eta} = \Lambda\frac{\partial}{\partial \eta}\left(c\Lambda\frac{\partial \phi}{\partial \eta}\right) + d \tag{40}$$

where

$$\Lambda = \frac{A\tan^2(1/A)\cos^2(\eta/A)}{2\tan(\eta/A)}$$

and

$$\bar{\Lambda} = \frac{A}{4}\sin(2\eta/A).$$

NUMERICAL SOLUTIONS AND ALGORITHM

Equation (40) is solved following a forward time-marching scheme and converting the differential equation as a difference equation with unequal intervals, using a central difference scheme for η and forward difference scheme for x. Thus (40) is transformed as

$$A_{i-1}\phi_{i-1}^k + B_{i-1}\phi_i^k + C_{i-1}\phi_{i+1}^k = D_{i-1},$$
$$i = 2, 3, \ldots, N-1 \tag{41}$$

where N denotes the number of grid points across the boundary layer. The expressions for A_{i-1}, B_{i-1}, C_{i-1} and D_{i-1} for velocity u and enthalpy h obtained from equations (36)–(40) are written as

$$A_{i-1} = [b\bar{\Lambda}\gamma' - c'\Lambda\gamma' - c\Lambda\bar{\gamma}']_i \tag{42}$$

$$B_{i-1} = \left[\frac{1}{\Delta x} + b\bar{\Lambda}\beta' - c'\Lambda\beta' - c\Lambda\bar{\beta}'\right]_i \tag{43}$$

$$C_{i-1} = [b\bar{\Lambda}\alpha' - c'\Lambda\alpha' - c\Lambda\bar{\alpha}']_i \tag{44}$$

$$D_{i-1} = \left[d + \frac{\phi_i^{k-1}}{\Delta x}\right]_i \tag{45}$$

where

$$c_i' = \alpha_i'(c\Lambda)_{i+1} + \beta_i'(c\Lambda)_i + \gamma_i'(c\Lambda)_{i-1}. \tag{46}$$

Defining

$$H1 = \eta_i - \eta_{i-1} \text{ and } H2 = \eta_{i+1} - \eta_i \tag{47}$$

α', β', γ' and $\bar{\alpha}'$, $\bar{\beta}'$, $\bar{\gamma}'$ are given in terms of $H1$ and $H2$ as

$$\alpha_i' = \frac{H1}{H2(H1+H2)}, \qquad \bar{\alpha}_i' = \frac{2}{H2(H1+H2)}$$
$$\beta_i' = \frac{H2-H1}{H1 \times H2}, \qquad \bar{\beta}_i' = \frac{-2}{H1 \times H2}$$
$$\gamma_i' = \frac{-H2}{H1(H1+H2)}, \qquad \bar{\gamma}_i' = \frac{2}{H1(H1+H2)}. \tag{48}$$

k denotes the grid points in the streamwise direction. As is clear from equations (41)–(46), to know ϕ_i^k, ϕ_i^{k-1} should be known. Thus ϕ_i^2 can be calculated only in terms of ϕ_i^1, and hence initial profiles for velocity and temperature are needed. In the present calculations, the profile given by Taylor *et al.* [16] is used, with very small values of boundary-layer thickness δ.

Equation (41) represents a system of equations with a tridiagonal matrix which can be solved easily by any standard method. The end points ϕ_1^k and ϕ_N^k are

determined from the boundary conditions at the wall and at the edge of the boundary layer as given by equations (23) and (24). u_∞ and T_∞ for equation (24) are obtained by numerically solving equations (25)–(28) by the fourth-order Runge–Kutta method.

The density variation is calculated from the relation

$$p = \rho_\infty T_\infty = \rho T \tag{49}$$

giving $\rho = \rho_\infty T_\infty / T$.

The normal coordinate y is computed using a fourth-order integration algorithm given by

$$y_i = y_{i-2} + (H1 + H2) \times \left[\frac{1}{6}\left(\frac{\partial y}{\partial \eta}\right)_i + \frac{2}{3}\left(\frac{\partial y}{\partial \eta}\right)_{i-1} + \frac{1}{6}\left(\frac{\partial y}{\partial \eta}\right)_{i-2}\right] \tag{50}$$

where

$$\frac{\partial y}{\partial \eta} = \frac{2\psi_E}{\rho u A}\frac{[1 + \lambda^2 \tan^2(1/A)]}{\tan(1/A)}. \tag{51}$$

NUMERICAL RESULTS AND DISCUSSIONS

The simultaneous system of algebraic equations (41), along with equations (42)–(51), is solved numerically on computer Cyber-730 system. The integration step in the x-direction is taken in such a way that it always satisfies the condition

$$\Delta x \leqslant \delta/2. \tag{52}$$

The number of grid points across the boundary layer are chosen so as to give a good description of the viscous layer. For the present calculation, 100 grid points are taken. But this number can vary between 50 and 150 depending upon the nature of the problem. For $N > 150$ or $N < 50$ oscillations of the solution appear, which could be due to computer round-off errors.

Numerical calculations are made for two characteristic conditions. The first case (a) deals with the supersonic flow of combustion product plasma used in open-cycle generators. Typical values are listed in Table 1. The second case (b) is for subsonic flow of argon–potassium plasma used in nonequilibrium generators, whose typical properties are listed in Table 2. Two values of wall temperature are considered to know its effects on the flow. The variation of viscosity and thermal conductivity is governed by the relations

$$\mu = 0.24137 + 0.75863T \tag{53}$$

$$k = 0.94777 - 3.58822T + 3.64045T^2 \tag{54}$$

as given by Rohatgi *et al.* [17] and

$$\beta_e \propto T^{1/2}, \qquad \beta_i \propto T^{1/2}. \tag{55}$$

The variation of electrical conductivity is taken as

$$\sigma = T^{11} \tag{56}$$

and

$$\sigma = \frac{T_e^{3/4}}{p^{1/2}} \exp\left[-12.5909\left(\frac{1}{T_e} - 1\right)\right] \tag{57}$$

Table 1. Typical properties of combustion MHD plasma

Gas	combustion products of hydrocarbon fuel in air
Seed	potassium = 2.0% (by weight)
Pressure	$P_0 = 3$ bar
Velocity	$U_0 = 1500\,\mathrm{m\,s^{-1}}$
Temperature	$T_0 = 2600\,\mathrm{K}$
Temperature at the wall	$T_w = 1500, 1250\,\mathrm{K}$
Magnetic flux density	$B_0 = 2\,\mathrm{T}$
Ratio of specific heats	$\gamma = 1.2$
Thermal conductivity	$k_0 = 0.18\,\mathrm{kg\,m\,s^{-3}\,K^{-1}}$
Electrical conductivity	$\sigma_0 = 11.5\,\mathrm{S\,m^{-1}}$
Viscosity	$\mu_0 = 9.625251 \times 10^{-5}\,\mathrm{kg\,m^{-1}\,s^{-1}}$
Molecular weight	$30\,\mathrm{kg\,kmol^{-1}}$
Length	2 m
Load parameter	0.6

Table 2. Typical properties of argon–potassium plasma

Gas	argon
Seed	potassium = 0.4% (by weight)
Pressure	$P_0 = 1$ bar
Velocity	$U_0 = 500\,\mathrm{m\,s^{-1}}$
Temperature	$T_0 = 2000\,\mathrm{K}$
Temperature at the wall	$T_w = 1500, 1250\,\mathrm{K}$
Magnetic flux density	$B_0 = 0.2$ T
Ratio of specific heats	$\gamma = 1.67$
Thermal conductivity	$k_0 = 7.60736 \times 10^{-2}\,\mathrm{kg\,m\,s^{-3}\,K^{-1}}$
Electrical conductivity	$\sigma_0 = 26.07211\,\mathrm{S\,m^{-1}}$
Viscosity	$\mu_0 = 9.74055 \times 10^{-5}\,\mathrm{kg\,m^{-1}\,s^{-1}}$
Molecular weight	$39.94\,\mathrm{kg\,kmol^{-1}}$
Length	2 m
Load parameter	0.5

for combustion product plasma and argon–potassium plasma respectively, where

$$T_e = 0.5T_g[1 + \sqrt{(1 + 0.00003966u^2U_0^2B_0^2)}] \tag{58}$$

as given in ref. [19].

With the above values of the parameters characterizing the flow, the variation of the velocity components u, v and temperature T in the boundary-layer region is obtained, as is discussed below.

Case (a)

The free-stream values of u, T and pressure gradient for the supersonic flow of the combustion product plasma are shown in Fig. 1. As is seen from the graph, the velocity decreases rapidly while the temperature increases slowly. The axial pressure gradient is positive and increases.

The profiles for u and T progressing along the streamwise direction are given in Figs. 2 and 3 for the two values of the wall temperature. The profiles get more and more curved as the flow progresses. There is no significant difference in the profiles when the wall temperature is reduced. The flow gradients increase marginally and the boundary-layer thickness decreases.

The variation of the skin friction coefficient c_f and the Nusselt number Nu is plotted in Figs. 4 and 5. Both c_f and Nu decrease as the flow progresses. When the wall temperature is reduced, the Nusselt number is reduced and the skin friction coefficient is increased.

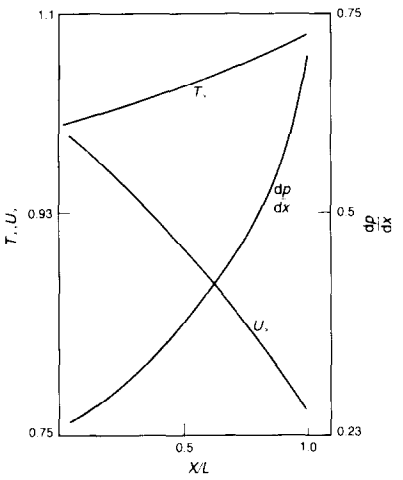

FIG. 1. Free-stream values of velocity, temperature and pressure gradient for combustion product plasma—case (a).

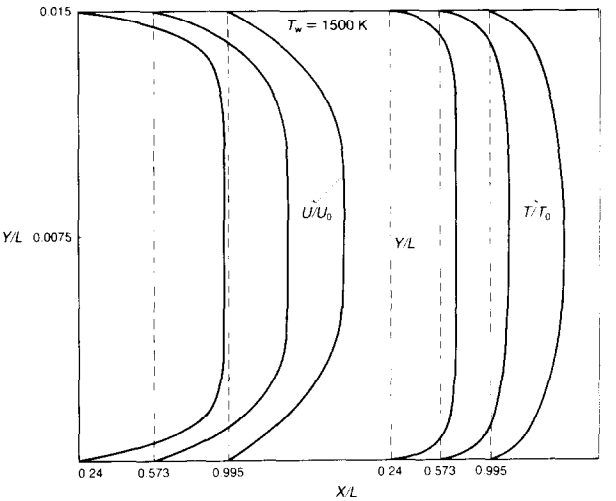

FIG. 2. Progress of the profiles of velocity and temperature for $T_w = 1500$ K for combustion product plasma—case (a).

But the effect of the wall temperature is more on the Nusselt number compared to its effect on the skin friction coefficient.

Since the generated power decreases as a result of the growth of the boundary layer, for any value of x, the generated power is more for $T_w = 1250$ K compared to $T_w = 1500$ K. Thus the losses due to the boundary layer are more compared to the effects of the reduced electrical conductivity due to wall temperature. With the decrease in the wall temperature, the flow separation can also be delayed as the skin friction coefficient is increased in this case.

Case (b)

The results of subsonic flow of argon–potassium plasma with nonequilibrium conductivity are plotted in Figs. 6–10. Figure 6 gives the free-stream values of the velocity temperature and pressure gradient. In this case, the velocity and negative pressure gradient increase while the temperature decreases. But as the interaction parameters and the Mach number are small, the variation is very slow.

Figures 7–10 show the behaviour of the flow variables with respect to axial distance and the wall temperature. The general characteristics remain the same as for the supersonic flow but the difference in the values of the skin friction and the Nusselt number for the two wall temperatures is more in this case.

A comparison of the supersonic and subsonic flows show that as a result of the heat friction or the conducted heat, the density decreases in the boundary layer, which leads to an increase in the boundary-layer thickness for the subsonic flows with the same Reynolds number. The transverse gradients of the flow variables decrease faster for the supersonic case compared to the subsonic flow.

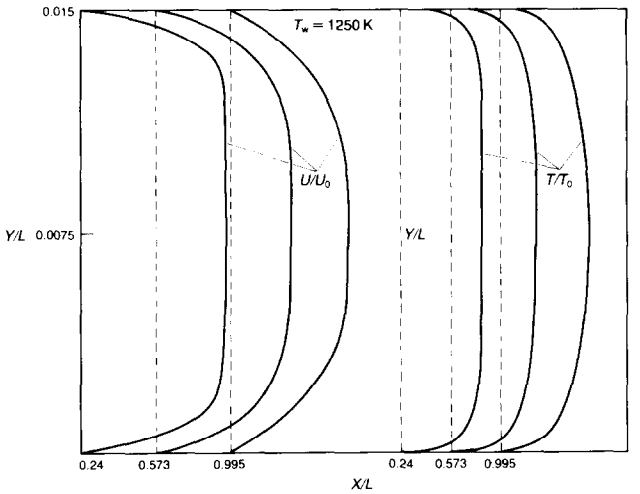

FIG. 3. Progress of the profiles of velocity and temperature for $T_w = 1250$ K for combustion product plasma—case (a).

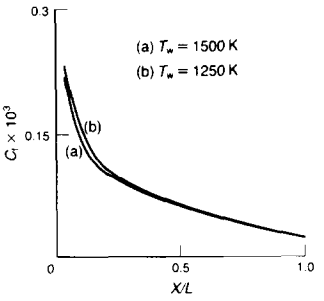

FIG. 4. Variation of skin friction coefficient for case (a) with T_w = 1500 and 1250 K.

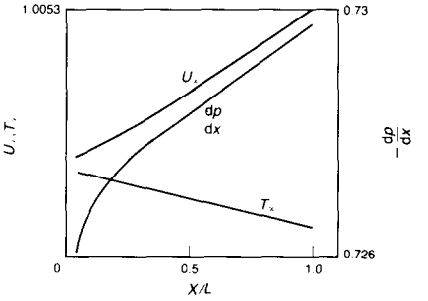

FIG. 6. Free-stream values of velocity, temperature and pressure gradient for argon–potassium plasma—case (b).

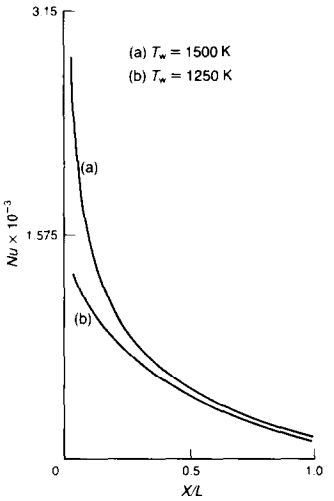

FIG. 5. Variation of Nusselt number for case (a) with T_w = 1500 and 1250 K.

Acknowledgement—This research was supported partially by the Department of Atomic Energy, Government of India.

REFERENCES

1. R. K. James and C. H. Kruger, Boundary layer profile measurements in the electrode wall of a combustion driven MHD channel, *17th Symposium on Engineering Aspects of MHD*, P.E. 3.1 (March 1978).
2. G. Dodel, Simultaneous measurements of the electron density and electron temperature distribution in a simulated Faraday type MHD generator, *5th Int. Conference on MHD Electrical Power Generation*, Vol. II, p. 127 (1971).
3. C. H. Kruger and S. L. Girshick, A review of MHD boundary layer research at Stanford, with emphasis on measurements of the effects of secondary flows, *8th Int. Conference on MHD Electrical Power Generation*, Moscow, Vol. 2, P.E. 5.1 (September 1983).
4. V. H. Blackman, M. S. Jones, Jr. and A. Demetriades, MHD power generator studies in rectangular channels, *Proc. Second Symposium on Engineering Aspects of Magnetohydrodynamics*, p. 180. Columbia University Press, New York (1962).
5. A. Maciulaitis and A. L. Loeffler, Jr., A theoretical investigation of MHD channel entrance flows, *A.I.A.A. Jl* **2**, 2100 (1964).
6. W. C. Moffatt, Analysis of MHD channel entrance flows using the momentum integral method, *A.I.A.A. Jl* **2**, 1495 (1964).
7. E. D. Doss, G. S. Argyropoulos and S. T. Demetriades, Two dimensional flow inside MHD ducts with transverse asymmetries, *A.I.A.A. Jl* **13**, 545 (1975).

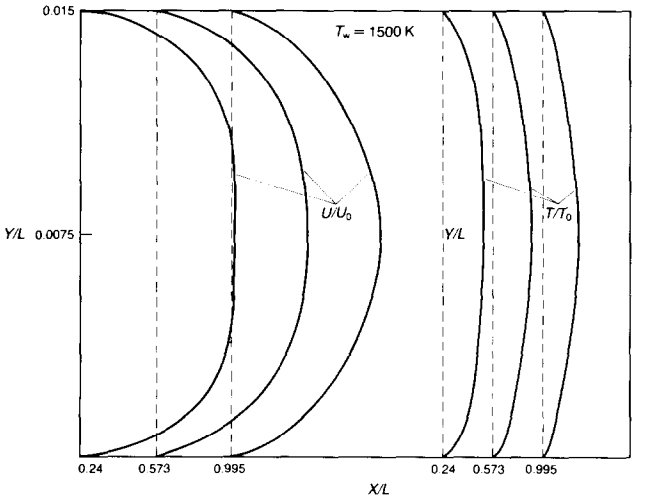

FIG. 7. Progress of the profiles of velocity and temperature for T_w = 1500 K for argon–potassium plasma—case (b).

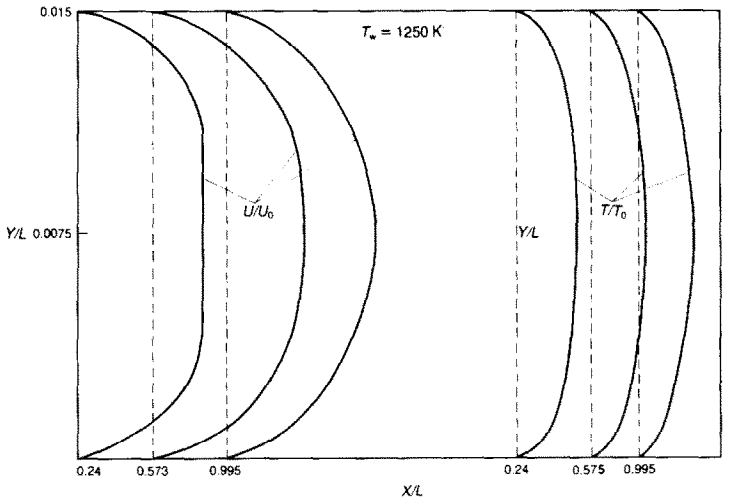

FIG. 8. Progress of the profiles of velocity and temperature for $T_w = 1250$ K for argon–potassium plasma—case (b).

8. J. Gertz, T. Opar, A. Solbes and G. Weyl, Modelling of MHD channel boundary layers using an integral approach, *18th Symposium on Engineering Aspects of MHD*, PB 4.1 (1979).
9. S. P. Vanka and R. K. Ahluwalia, Three dimensional flow and thermal development in magnetohydrodynamic channels, *J. Energy* **6**, 218 (1982).

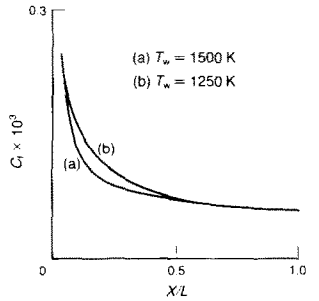

FIG. 9. Variation of skin friction coefficient for case (b) with $T_w = 1500$ and 1250 K.

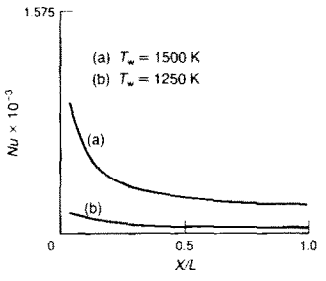

FIG. 10. Variation of Nusselt number for case (b) with $T_w = 1500$ and 1250 K.

10. S. V. Patankar, V. S. Pratap and D. B. Spalding, Prediction of laminar flow and heat transfer in helically coiled pipes, *J. Fluid Mech.* **62**, 539 (1974).
11. S. V. Patankar and D. B. Spalding, *Heat and Mass Transfer in Boundary Layers*, 2nd edn. Intertext, London (1970).
12. E. Arad, M. Berger, M. Israeli and M. Wolfstein, Numerical calculation of transitional boundary layer, *Int. J. numer. Methods Fluids* **2**, 1 (1982).
13. A. M. Dhanak, Heat transfer in magnetohydrodynamic flow in an entrance section, *J. Heat Transfer* **87**, 231 (1965).
14. W. H. Heiser and W. J. Boronhorst, A modified Pohlhausen velocity profile for MHD boundary layer problems, *A.I.A.A. Jl* **4**, 1139 (1966).
15. G. W. Sutton and A. Sherman, *Engineering Magnetohydrodynamics* McGraw-Hill, New York (1965).
16. R. E. Taylor, Y. C. L. Wu and D. L. Denzel, Effects of boundary layers upon current distribution and internal resistance in segmented magnetohydrodynamic channels, *J. appl. Phys.* **42**, 2689 (1971).
17. V. K. Rohatgi, N. Venkataramani, R. Jayakumar, A. K. Das and V. R. Ramaprasad, Comparison of gasified coal for MHD power generation, *Proc. 6th Int. Symposium on MHD Power Generation*, Vol. 1, p. 45 (1975).
18. M. Berger, M. Israeli and M. Wolfshtein, *Numerical Solution of Transitional Boundary Layers, Simulation of Systems '79*, p. 437. North-Holland, Amsterdam (1980).
19. G. Paran Gowda, M. L. Mittal, G. P. Gupta and V. K. Rohatgi, Effects of ionisational non-equilibrium on the electron density across the nonequilibrium MHD channel, *Energy Res.* **8**, 263 (1984).
20. L. L. Lengyel, Two-dimensional current distributions in Faraday type MHD energy converters operating in the non-equilibrium conduction mode, *Energy Conv.* **9**, 13 (1969).

ECOULEMENT ET TRANSFERT THERMIQUE DANS LE CANAL D'UN GENERATEUR DE PUISSANCE MHD

Résumé—On obtient une solution numérique des équations gouvernant l'écoulement d'un gaz compressible, visqueux, conducteur électrique, à propriétés variables, en présence d'un champ magnétique uniforme. Les distributions de vitesse et de température sont analysées pour des écoulements subsoniques et supersoniques tels qu'ils sont réalisés dans un générateur MHD.

STRÖMUNG UND WÄRMEÜBERGANG IN EINEM MHD-GENERATOR

Zusammenfassung—Die Grundgleichungen für die Strömung eines elektrisch leitenden, zähen, kompressiblen Gases mit nichtkonstanten Stoffeigenschaften werden für den Fall gelöst, daß ein gleichmäßiges Magnetfeld der Gasströmung überlagert ist. Dabei werden Geschwindigkeits- und Temperatur-Verteilung bei Unter- und Überschall-Strömung in einem MHD-Generator untersucht.

ТЕЧЕНИЕ ГАЗА И ТЕПЛОПЕРЕНОС В КАНАЛЕ МГД-ГЕНЕРАТОРА

Аннотация—Получено численное решение уравнений, описывающих течение электропроводного вязкого сжимаемого газа с переменными свойствами в однородном магнитном поле. Анализируются распределения скорости и температуры при дозвуковых и сверхзвуковых течениях в канале МГД-генератора.